Effect of Microstructural Degradation on Crack Tip Stress Fields in Two-Phase Single Crystals

E.P. Busso, N.P. O'Dowd, S. Dumoulin, and D. Allen†

Department of Mechanical Engineering
Imperial College, London, UK
† ALSTOM Power Technology Centre, Whetstone, UK

ABSTRACT

A large proportion of the service life of high temperature single crystal components is taken up in initiating and growing surface cracks, which are driven by thermally induced stresses and environmental effects. In this work, the effect of a reduction in the volume fraction of the γ' precipitate phase in Ni-base superalloys on the time-dependent crack tip stresses is analysed numerically. Such variations can be related to the microstructural degradation caused by oxidation and diffusion processes around surface cracks in superalloy single crystals. The approach relies on a recently proposed multi-scale rate-dependent crystallographic theory to describe the macroscopic constitutive behaviour of the single crystal in terms of material parameters which depend explicitly on the characteristics of the precipitate phase at the microscale.

Results of a finite element study on a typical compact tension specimen reveal a strong dependency of the local crack tip stresses and strains on the local volume fraction of the precipitate population. The implications of these findings in relation to the microstructural degradation caused by oxidation at crack faces are discussed.

KEYWORDS

Single crystals; Superalloys; Oxidation; Crack Growth; Fracture.

INTRODUCTION

In two-phase single crystals such as Ni-base superalloys, heterogeneities exist at both the microscopic and mesoscopic levels. At the microscale, they are introduced by the presence of the 0.5-1 μm γ' precipitates and can become more pronounced due to the changing morphology of the precipitates during service and to inhomogeneous deformation patterns. At the mesoscale, e.g. in 10–100 μm sized regions, the presence of surface cracks also introduces a degree of heterogeneity in the local microstructure as a result of the local microstructural degradation caused by the oxidation of the crack faces [1][2].

Conventional single crystal models are unable to predict the effects of such heterogeneities as they generally treat the material as a homogeneous single crystal solid whose mechanical behaviour is uncoupled from inter-diffusion and oxidation processes. It is well known, however, that local variations in precipitate volume fraction strongly affect the local material behaviour. Although much work has been done to explain such volume fraction effects, it was not until recently that they were quantified for a range of temperature and strain rate conditions using periodic unit-cell techniques [3][4]. The results have been incorporated into a state variable crystallographic formulation to account for experimentally observed precipitate size and volume fraction effects in a Ni-base superalloy [5].

The main objective of this work is to quantify the effect of the reinforcing phase on the stress and strain fields at crack tip regions and to enhance the current understanding of the factors controlling short crack behaviour in Ni-base superalloys at high temperatures. The structure of the paper is as follows. First, a brief outline of the constitutive approach is presented. Then, the crack tip fields in a typical compact tension (CT) specimen are presented as a function of the volume fraction of the precipitate population. This is followed by a discussion of the results and the implications for crack growth predictions in single crystals.

MULTI-SCALE CRYSTALLOGRAPHIC FORMULATION

The average macroscopic stress-strain behaviour of the superalloy single crystal (SC) of interest, viz. CMSX4, is described by the multi-scale rate dependent crystallographic formulation recently proposed by Busso [5]. The flow rule relies on a stress-dependent activation energy expressed in terms of two internal state variables per slip system, α: a macroscopically average slip resistance S^α, and a internal or back stress B^α. Thus,

$$\dot{\gamma}^\alpha = \dot{\gamma}_o \exp\left[-\frac{F_o}{k\theta}\left\langle 1 - \left\langle \frac{|\tau^\alpha - B^\alpha| - S^\alpha \mu/\mu_0}{\hat{\tau}_0 \mu/\mu_0} \right\rangle^p \right\rangle^q \right] sgn(\tau^\alpha) \; , \tag{1}$$

where τ^α is the resolved shear stress, θ the absolute temperature, μ, μ_0 the shear moduli at θ and 0 K, respectively, and F_0, $\hat{\tau}_o$, p, q and $\dot{\gamma}_0$ are material parameters.

The evolutionary behaviour of the overall slip resistance is given by,

$$\dot{S}^\alpha \;=\; \sum_{\beta=1}^{n} \delta_S^{\alpha\beta} \left[h_s - d_D (S^\beta - S_0^\beta) \right] |\dot{\gamma}^\beta| \; , \tag{2}$$

where S_0^α is the initial value of S^α, d_D is a dynamic recovery function and n is the total number of slip systems. In Eq. 2, $\delta_S^{\alpha\beta}$ is the latent hardening or interaction function. Here, self-hardening is assumed so that $\delta_S^{\alpha\beta} = \delta_{\alpha\beta}$, the Kroneker delta.

The formulation contains an explicit link between the γ' precipitate population at the microscale and the behaviour of the homogeneous equivalent material at the macroscale. This link is introduced through the dynamic recovery function d_D and the initial microstructural state, S_0^α in Eq. 2 which, in turn, depend on the characteristics of the current precipitate population. Here,

$$d_D \;=\; \hat{d}_D \left\{ l/l_m, \, \mathrm{v}_f \right\} \quad , \tag{3}$$

$$S_0^\alpha \;=\; \hat{S}_0 \left\{ l/l_m, \, \mathrm{v}_f \right\} \quad , \tag{4}$$

where l/l_m is the precipitate size normalised by a mean reference value, and v_f the precipitate volume fraction. Equations 3 and 4 have been calibrated from FE analyses of periodic unit cells at the microscale containing the individual precipitates [4]. Note that the effects of the precipitate aspect ratio will not be quantified in this paper. For details, see [3] and [4].

The back stress evolves according to ,

$$\dot{B}^\alpha \;=\; h_B \dot{\gamma}^\alpha - r_D B^\alpha |\dot{\gamma}^\alpha|, \tag{5}$$

where h_B is the hardening coefficient, and r_D a dynamic recovery function expressed in terms of the current overall deformation resistance,

$$r_D \;=\; \frac{h_B \, \mu_o}{S^{(\alpha)}} \left\{ \frac{\mu_0'}{f_c \lambda} - \mu \right\} \; . \tag{6}$$

Here, f_c and λ are statistical factors, and μ_0' is the shear modulus in the slip plane. Note that the dependency of the back stress on the characteristics of the precipitate population is implicitly incorporated through S^α in Eq. 6.

The above crystallographic formulation has been implemented numerically into a material subroutine in a commercial FE code [6] using a large strain algorithm with an implicit time-integration procedure. It relies on the multiplicative decomposition of the total deformation gradient, $\mathbf{F}$, into an inelastic component, $\mathbf{F}^p$,

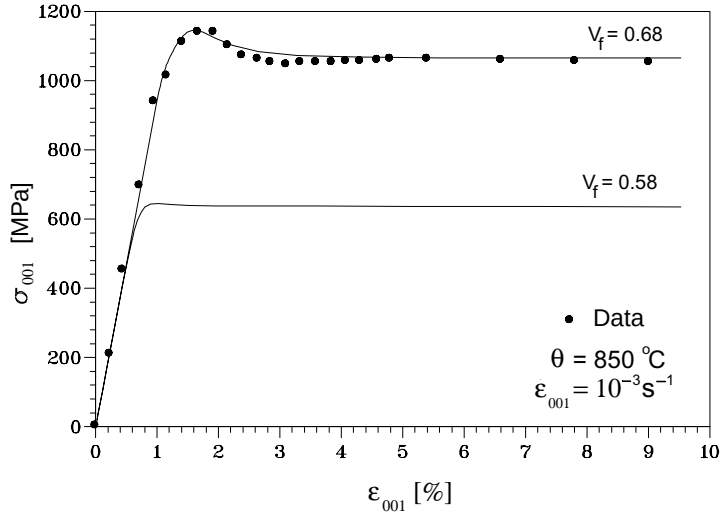

Figure 1: Effect of precipitate volume fraction on the $< 001 >$ monotonic response of CMSX4 at 850°C and 10^{-3} 1/s. Symbols represent experimental data for the $V_f = 0.68$ case

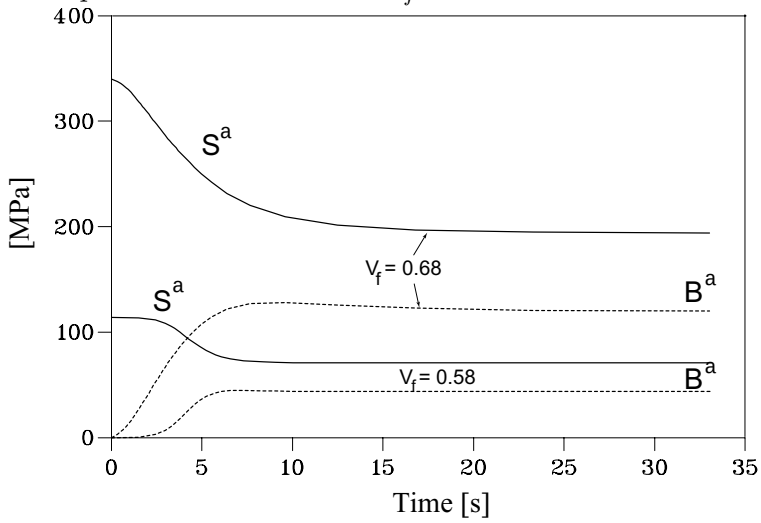

Figure 2: Predicted effect of the evolutionary behaviour of the $\{111\} < 011 >$ internal slip system variables for the monotonic stress-strain curves shown in Fig. 1

associated with pure slip, and an elastic component, $\mathbf{F}^e$, which accounts for the elastic stretching and rigid-body rotations. Thus, $\mathbf{F} = \mathbf{F}^e\mathbf{F}^p$. For details, refer to [4],[5].

The model calibration was carried out with the twelve octahedral ($\{111\} < 011 >$) and six cubic ($\{100\} < 011 >$) slip systems considered to be potentially active. The reference data to calibrate the model for $\mathrm{v}_f = 0.68$ were obtained from uniaxial monotonic, cyclic and creep tests, and, the data for $\mathrm{v}_f < 68\%$ from periodic unit cell analyses (see [3],[4]).

Typical predictions of the monotonic uniaxial behaviour of CMSX4 at 850°C and 10^{-3} 1/s are shown in Fig. 1 for two different γ' volume fractions, namely 58 and 68%, together with experimental data for the latter case. Figure 1 shows that a 10% reduction in volume fraction results in a 40% decrease in the superalloy steady state flow stress at this temperature and strain rate. The corresponding evolutionary behaviour of the internal slip system variables for each of the eight active (and equally stressed) $\{111\} < 011 >$ systems is shown in Fig. 2. The correspondence between the macroscopic softening and hardening behaviour and the steady state values of the slip resistance and the back stress can be clearly inferred from Figs. 1 and 2. For instance, the macroscopic softening observed for $\mathrm{v}_f = 0.68$ is associated with a large decrease in the slip resistance, from its initial value of 338 MPa to its steady state value of 201 MPa. Even though a similar S^α softening trend is seen for $\mathrm{v}_f = 0.58$, the macroscopic effect is negligible (see Fig. 1).

FINITE ELEMENT MODELLING

The three dimensional finite element mesh used to analyse the crack tip deformation of a typical compact tension specimen is shown in Fig. 3. A crack length of $a = 15.6$ mm and a crack length-to-specimen width ratio of $a/W = 0.6$ were used. Here, the specimen thickness and height are 12.5 mm and 31.2 mm, respectively, and the notch radius is 1.3 μm.

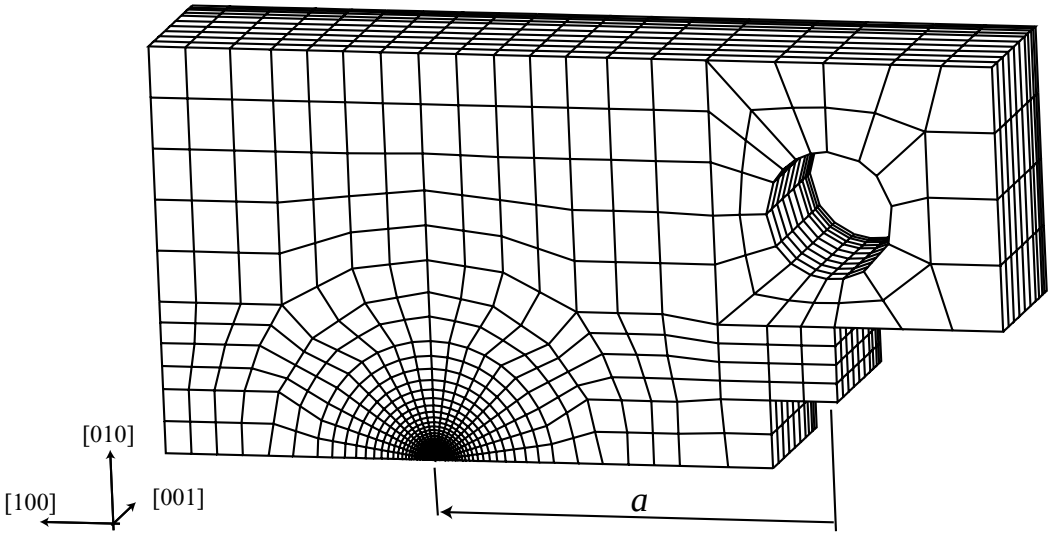

Figure 3: Finite element mesh of the CT specimen

The plane of the specimen is normal to the [001] crystallographic axis and the crack faces lie normal to the [010] axis. Note also that, due to the symmetries of the lattice and the specimen, only 1/4th of the specimen needs to be modelled. In total, 14000 linear brick elements are used in the analysis, with a focused mesh at the crack tip. The smallest element size in the model is 1.0 μm (or $\sim 6 \times 10^{-5} a$).

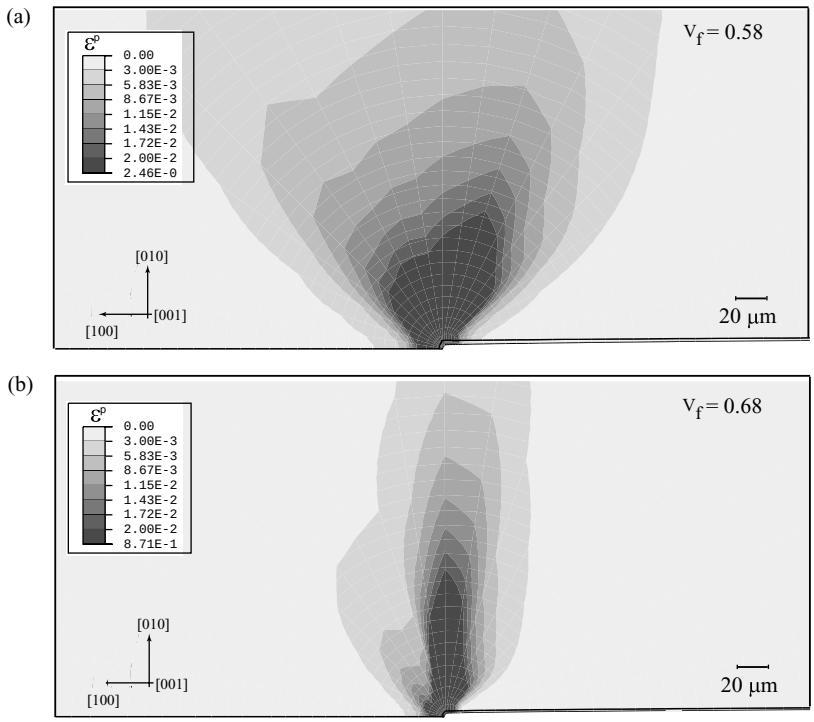

Figure 4: Contours of accumulated inelastic strain near the notch tip for: (a) 58% and (b) 68% γ' volume fraction after 320 hours exposure at 850°C

RESULTS AND DISCUSSIONS

The results to be discussed in this section are for CT specimens with a fixed content and uniform distribution of precipitates. Two cases are examined: an alloy with a precipitate volume fraction of 68%, which corresponds to that of CMSX4 at the start of life, and an alloy with a volume fraction of 58%, which is a typical volume fraction found near crack faces after long-term exposure to an oxidising environment. In on-going work, the effect of time and spatial evolution of the γ' volume fraction and size on the deformation and stress state is being studied.

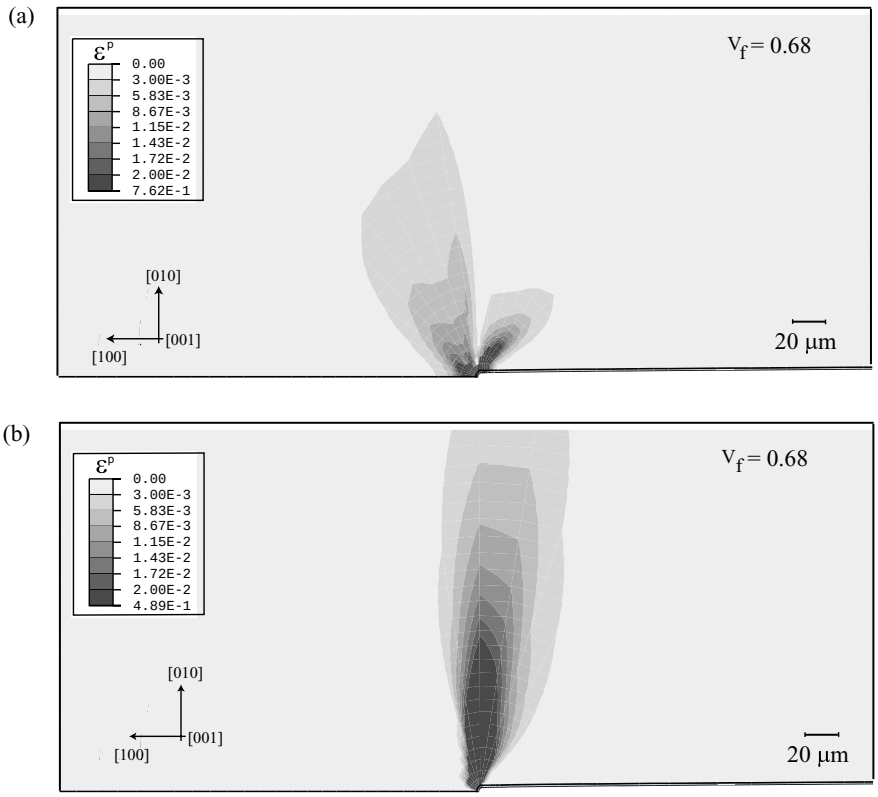

Figure 5: Contributions to the overall accumulated inelastic strain around the notch tip from the (a) octahedral and (b) cubic slip systems for the $v_f = 0.68$ case shown in Fig. 3

Figures 4 to 6 show results for the CT specimen loaded with a stress intensity factor of 10 MPa $\sqrt{m}$ at 850 °C. In Fig. 4, contours of accumulated inelastic strain are presented for (a) $v_f = 58\%$ and (b) $v_f = 68\%$ after 320 hours exposure. The contours are shown at the central notch root region of the specimen where fracture is expected to initiate. It is worth noting the greater magnitude and extent of the accumulated overall slip for the $v_f = 58\%$ case, which is a considerably softer material (see Fig. 1). The contributions to the overall accumulated inelastic strain around the tip of the sharp notch for the $v_f = 68$ % case (see Fig. 4(b)) from the octahedral and cubic slip system families are shown in Figs. 5 (a) and (b), respectively. Since the specimen is loaded along the [010] direction, one would expect the octahedral slip systems to be dominant, as it is the case under uniaxial $< 001 >$ (homogeneous) deformation. However, Fig. 5 reveals that the contribution from the cubic slip systems is equally important. This is a result of the multiaxial nature of the stress distribution near the notch region.

In Figs. 6(a) and (b), the distribution of the stress component normal to the crack faces, σ_{010}, and the mean hydrostatic stress, $\sigma_h = (\sigma_{100} + \sigma_{010} + \sigma_{001})/3$, respectively, are given in terms of the distance from the tip of the notch and the γ' volume fraction. The peak normal stress in Fig. 6(a), found at approximately 23 μm from the sharp notch root, decreases by 34% for a 10 % decrease in the precipitate volume fraction. Thus, the crack driving force for cleavage fracture is considerably reduced. It is known that the rate of growth of voids within the single crystal at high temperatures depends on the magnitude of σ_h and the local slip rates. Therefore, from the results of Figs. 4 and 6(b), the evolution of ductile damage could be inferred.

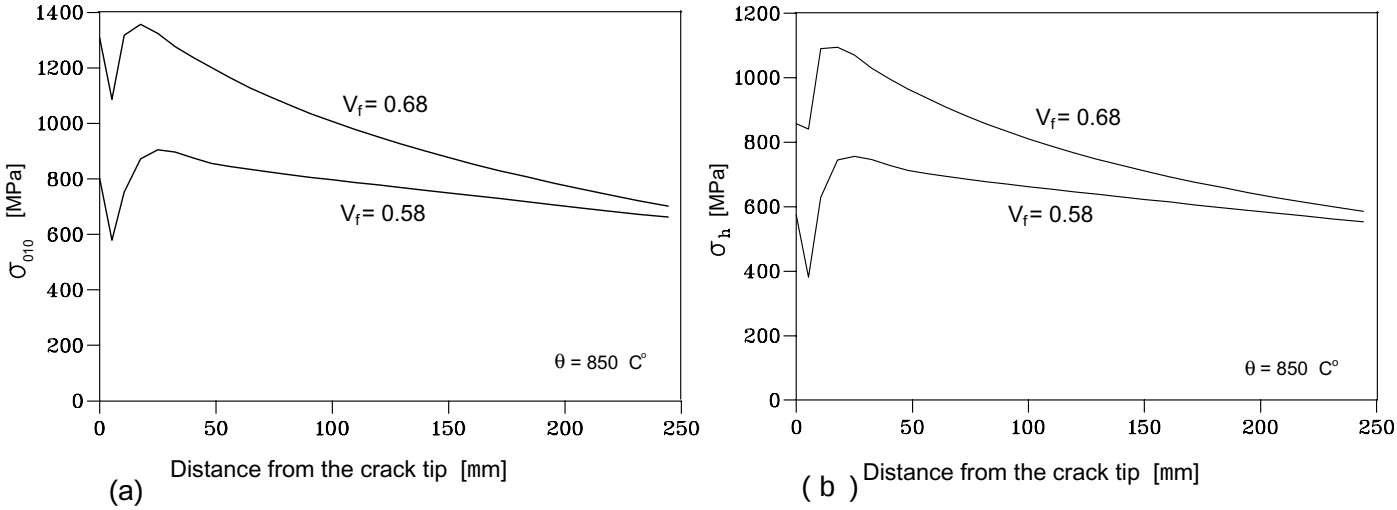

Figure 6: Distribution of (a) the stress component normal to the crack faces and (b) the mean hydrostatic stress (= $(\sigma_{100} + \sigma_{010} + \sigma_{001})/3$), as a function of the distance from the tip of the notch and the γ' volume fraction

In on-going work, parametric studies of the type shown here coupled with oxygen diffusion from the environment into the crack faces are being conducted and the resulting information used to formulate appropriate fracture mechanics-based formulation for crack growth predictions under creep-fatigue interaction.

CONCLUDING REMARKS

This work has shown that, in single crystal alloys reinforced with a high precipitate volume fraction, such as Ni-base superalloys, the decrease in the precipitate content due to environmental effects can have a strong effect on the local stresses responsible for both cleavage and stable crack growth. Such effects must be incorporated into fracture-mechanics based crack growth models to assure the accuracy of hot section component life assessments.

ACKNOWLEDGEMENTS

Financial support for this work by the EPSRC (UK) through grant GR/N12312 and by Alstom Power (UK) are gratefully acknowledged. The authors are grateful to Dr. F. Andrieux for her assistance in the calibration of the crystallographic model.

References

[1] Andrieu, E. and Pineau, A. (1999), Study of the Coupled Phenomena Involved in the Oxidation Assisted Intergranular Cracking in Ni-Base Superalloys, *J. de Physique IV*, V. 9 , pp. 3-12.

[2] Martinez-Esnaola, J.M., Martin-Meizoso, A., Affeldt, E.E., Bennett, A. and Fuentes, M. (1997), High Temperature Fatugue in Single Crystal Superalloys, *Fatigue Fract. Engng. Mater. Struct.*, V. 20 , pp. 771-788.

[3] Busso, E.P., Meissonnier, F., and O'Dowd, N.P. (2000), Gradient-Dependent Visco-Plastic Deformation of Two-Phase Single Crystals. *J. Mechanics Physics Sol.*, V. 48 , pp. 2333-2361.

[4] Meissonnier, F., Busso, E.P., and O'Dowd, N.P. (2001), Finite Element Implementation of a Non-Local Visco-Plastic Crystallographic Formulations. *Int. Journal of Plasticity*, V. 17, pp. 601-640.

[5] Busso, E.P., A Crystallographic Formulation for Superalloy Single Crystals with Explicit Microstructural Length Scales. Part I: Model Formulation. Submitted for publication.

[6] ABAQUS V. 5.8 (1999), Hibbitt, Karlsson and Sorensen Inc., Providence, RI.